Quantitative proteomics and dynamic imaging reveal that G3BP-mediated stress granule assembly is poly(ADP-ribose)-dependent following exposure to MNNG-induced DNA alkylation

Maxim Isabelle[1], Jean-Philippe Gagné[1], Imed-Eddine Gallouzi[2] and Guy G. Poirier[1,*]

[1]Centre de recherche du CHUQ, Laval University, Cancer Department, Québec, Canada
[2]Department of Biochemistry, McGill University, Montréal, Québec, Canada
*Author for correspondence (guy.poirier@crchul.ulaval.ca)

Accepted 20 May 2012
Journal of Cell Science 125, 4555–4566

doi: 10.1242/jcs.106963

Summary

Poly(ADP-ribose) (pADPr) is a heterogenic molecule synthesised from NAD by poly(ADP-ribose) polymerases (PARPs). Many cellular functions from genome integrity surveillance, cell cycle progression and DNA repair to apoptosis are affected by pADPr through its network of associated proteins. Using quantitative proteomics, we established a temporal map of pADPr-associated complexes upon genotoxic stress. Results suggested a strong pADPr association to many proteins involved in stress granule formation, notably the ras-GAP SH3-binding protein G3BP, as well as in the later phases of alkylation-stress-induced responses. Further investigation with dynamic imaging clearly demonstrated a pADPr-dependent initiation of stress granule assembly originating from the nucleus. The co-transfection of G3BP with poly(ADP-ribose) glycohydrolase (PARG) indicates that pADPr is involved in modulating the nuclear translocation of G3BP. Moreover, a peptide pADPr blot assay of G3BP revealed that pADPr binds to the glycine–arginine-rich domain of G3BP. Thereafter, we established a comprehensive G3BP interactome in the presence of pADPr. Our findings establish a novel function for pADPr in the formation of G3BP-induced stress granules upon genotoxic stress.

Key words: pADPr, G3BP, Stress granules, SILAC, Quantitative proteomics

Introduction

Following genotoxic insult, DNA strand breaks are rapidly detected by poly(ADP-ribose) polymerases (PARPs) that then synthesize a heterogeneous polymer assembled from ADP-ribose moieties ranging from a few to more than 300 units. Shortly after their formation, the poly(ADP-ribose) polymer (pADPr) begins to degrade due to the rapid action of poly(ADP-ribose) glycohydrolase (PARG). The interplay between PARP and PARG is responsible for the transient and dynamic nature of the pADPr. PARPs also modulate multiple processes within the cell not only by post-translationally modifying proteins through poly(ADP-ribosyl)ation but also by generating free pADPr (through PARG activities), which is thought to act as a signalling messenger (D'Amours et al., 1999). Poly(ADP-ribosyl)ation has been linked to DNA-related processing and chromatin modulation (Tulin and Spradling, 2003; Rouleau et al., 2004; Kim et al., 2005). Regulation by pADPr is found in a wide range of biological processes such as DNA damage response, apoptosis, chromatin remodelling, transcriptional regulation and epigenetics (reviewed by Hassa and Hottiger, 2008). In the established model of PARPs (PARP-1/-2)-mediated DNA-dependent activation upon genotoxic stress, the recognition of damaged DNA strand breaks stimulates their auto-poly(ADP-ribosyl)ation and the trans-poly(ADP-ribosyl)ation of histones and other proteins (Lindahl et al., 1995; Amé et al., 1999). The local accumulation of pADPr acts as a loading platform for the recruitment of chromatin remodelling and DNA repair factors. The dynamics of the system is derived from both the contribution of pADPr-synthesising PARPs and pADPr catabolism by PARG (Rouleau et al., 2010) and generates a transient accumulation of pADPr in the nucleus. During mild genotoxic stress, pADPr supports cell survival by activating key pathways in DNA repair response. However, when extensive damage occurs, the massive accumulation of pADPr can trigger apoptosis-like cell death (parthanatos) (Wang et al., 2009) or necrotic cell death as a consequence of cellular energy depletion. Therefore, the level of pADPr that is determined by the relative enzymatic activities of PARPs and PARG represents an important modulator of cell fate.

Although the exact mechanism by which pADPr can relay information from the nucleus to extra-nuclear compartments remains elusive, the pADPr-dependent translocation of apoptosis inducing factor (AIF) from the mitochondria to the nucleus supports the idea of a nucleo-cytoplasmic shuttling of pADPr. Using proteomics strategies, our laboratory has previously shown that PARG is resident in mRNPs (Gagné et al., 2003) and that many of the heterogeneous nuclear ribonucleoproteins (hnRNPs) are pADPr-binding proteins (Gagné et al., 2008). Recently, Leung and colleagues reported that specific PARPs and PARG isoforms associate with cytoplasmic messenger ribonucleoprotein (mRNP) complexes and that pADPr is required for the assembly

Journal of Cell Science

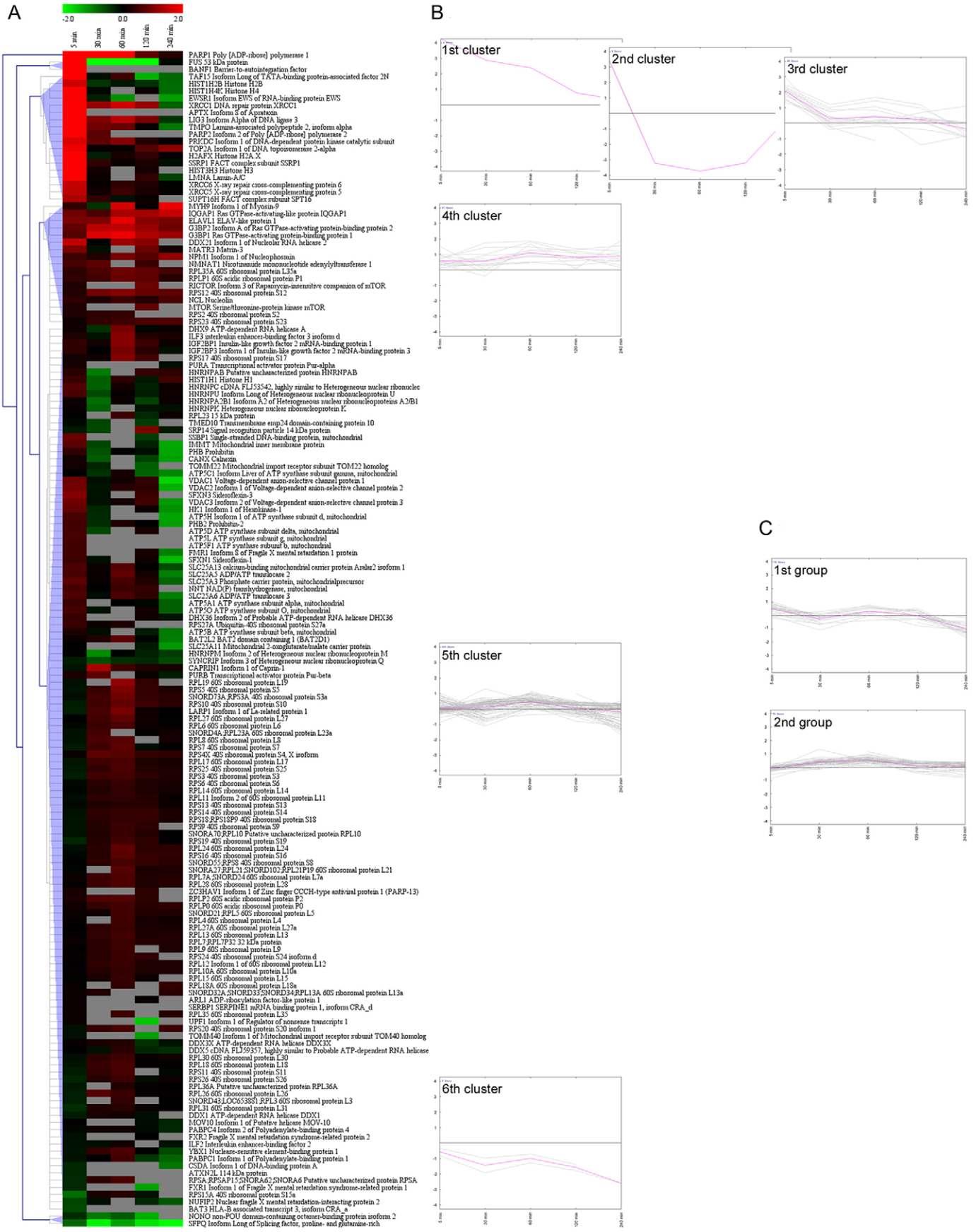

Fig. 1. See next page for legend.

of stress granules (SGs) (Leung et al., 2011). SGs are mRNP particles that assemble in response to a variety of stresses, conditions during which translation initiation is significantly impaired. SGs recruit translationally stalled mRNAs and typically 40S ribosome proteins, eukaryotic initiation factors (eIFs), poly(A)-binding proteins (PABP) and several RNA-binding proteins (Kedersha et al., 2005; Anderson and Kedersha, 2009). One of the main functions of SGs is to recruit key cellular mRNAs to prevent their translation and protect them from decay. However, as soon as the stress is relieved, the mRNAs are sent back to the translation machinery to be translated. SG formation depends on various factors such as the ras-GAP SH3-binding protein G3BP and eIF3 as well as the mRNAs they recruit (Kedersha and Anderson, 2002). In contrast, disassembly correlates with recovery of protein synthesis as a result of the reinitiation of mRNA translation. Therefore, SGs can be viewed as a vessel for the reprogramming of the cellular translation machinery that favours the expression of housekeeping genes needed during the response to various stresses.

While the pADPr protein ligands have been identified by a high-throughput mass spectrometry analysis of cells exposed to genotoxic stress (Gagné et al., 2008), we still do not know whether and how these associations are modulated during the stress response. In this paper, we address these questions by using quantitative proteomics to analyse the composition of pADPr-associated proteins at different times after DNA-damage. Stable isotope labelling by amino acids in cell culture (SILAC)-based analysis established a temporal profile of pADPr-associated proteins that goes beyond the initial DNA damage response. Interestingly, we found that G3BP, one of the components of the SG assembly, was enriched in pADPr-containing protein complexes at later time points following alkylation-induced DNA damage and PARP activation. We demonstrate that G3BP is a non-covalent pADPr-binding protein *in vitro* and that it associates with pADPr and pADPr-binding proteins *in vivo*. A peptide screening strategy revealed that G3BP possesses a non-covalent pADPr-binding motif in its C-terminal glycine-arginine-rich region. In addition, we show that G3BP-containing cytoplasmic foci assemble in a pADPr-dependent manner and that these foci originate from a nuclear pADPr synthesis signal. Finally, the colocalization of G3BP aggregates with SG markers and other proteins provides insights on the possible nucleocytoplasmic shuttling mechanism of pADPr. Taken together, these data indicate an important connection between the formation of G3BP-induced stress granules and the cellular response to genotoxic stress mediated by PARPs.

Results

Temporal proteomics profile of pADPr-associated proteins

We used quantitative temporal proteomics to uncover new information about the dynamics of pADPr-associated protein complexes upon PARP activation following alkylation-induced DNA damage especially at later time-points. The label-free SILAC approach (reviewed by Ong and Mann, 2007; Harsha et al., 2008) appeared most appropriate to address the highly dynamic nature of pADPr in cell cultures as the early incorporation of the isotope label minimizes the number of manipulations and provides almost 100% labelling efficiency (Iliuk et al., 2009).

To induce DNA alkylation and PARP activation, ~40 million HeLa cells (6×15 cm pooled dishes) per conditions, were exposed to methyl-N′-nitro-N′-nitrosoguanidine (MNNG). These experiments were performed in triplicate. The time course represents HeLa cells subjected to MNNG incubation from 5 up to 60 min followed by a recovery for the last two points (120 and 240 min). Therefore, the time-points indicate the time during which cells were exposed and recover from stress-induced genotoxic alkylation damage. Thereafter, total extracts were subjected to pADPr pull-down followed by high-throughput mass spectrometry. Using stringent selection criteria, described in the Bioinformatics section of the Materials and Methods, 163 proteins were identified. These proteins were identified in at least two out of three experiments with a minimum of two unique peptides in agreement with ProteinPilot4 parameters described in Materials and Methods (supplementary material Table S1). The identification criteria also allowed us to determine the relative quantity of each protein with a high degree of confidence. SILAC ratios were reported with time-point zero (untreated cells) as the baseline over each other of the 5 time points analysed following MNNG-induced genotoxic stress (5, 30, 60, 120 and 240 minutes). SILAC ratios obtained were considered significantly different when below 0.8 and higher than 1.2. For example, the PARP-1 ratio after 5 minutes of MNNG incubation is ~19 ($\log_2$ 4.26), indicating that PARP-1 is 19 times more abundant in pADPr-containing protein complexes at the peak of pADPr synthesis compared to basal control conditions (Fig. 1A). SILAC ratios were transformed into $\log_2$ ratios to facilitate interpretation. Actually, ratio measurements are most naturally processed in the log space (use of $\log_2$ for simplicity). Indeed, with the $\log_2$ values, a 2-fold increase and 2-fold decrease are symmetric around zero making visualisation of results easier. Clustering of these proteins was performed according to their pADPr-association characteristics over time. The K-means method was applied since this kind of clustering offers the possibility to group complex time course expression data into a pre-selected number of distinct clusters according to their similarity (Albaum et al., 2011). Six K-means clusters were estimated to be the smallest number of resulting clusters with clearly distinguishable association profiles (Fig. 1A).

The first three clusters are characterised by pADPr-associated proteins with very high ratios after 5 minutes of MNNG incubation (Fig. 1B). The first cluster is uniquely represented by PARP-1 which displays very high ratios up to 120 min following initial activation. The second cluster includes the PARP-1 interacting protein BANF1 (Montes de Oca et al., 2009) and FUS, a DNA-binding protein that may play a role in the maintenance of genomic integrity (Sugawara et al., 2010). BANF1 and FUS dramatically accumulated at 5 min compared to basal conditions. The third cluster included major proteins of the base excision repair (BER) pathway (XRCC1, DNA ligase III), nonhomologous end-joining (NHEJ) (DNA-PK, Ku70, Ku80) and several chromatin-associated proteins such as the FACT complex subunits SUPT16H and SSRP1. This cluster also

Fig. 1. Hierarchical clustering of SILAC ratios. (**A**) Profiles of protein complexes were clustered according to the $\log_2$ ratio and displayed as a heat map where green represents negative and red positive values corresponding to the scale bar. (**B**) Centroids graph representing profiles of various proteins belonging to one of the six clusters that are indicated in the top left corner. In each cluster, pale grey lines indicate the ratio for each protein and the pink line represents the mean variation for the cluster. The *y*-axis is the $\log_2$ ratio and the *x*-axis the MNNG time points (in minutes). (**C**) Extracted centroid graphs of the fifth cluster subdivided in two subgroups.

included PARP-2, some core histones (H2AX, H2B, H3, H4) and nuclear lamina-associated proteins such as the lamin A/C and thymopoeitin (TMPO), which participates in chromatin organisation. Globally, the three first clusters bring together a variety of chromatin remodelling and DNA damage signalling/repair factors consistent with the transient accumulation of pADPr at DNA damage sites.

The fourth cluster peaked 60 min after MNNG-induced genotoxic insult (Fig. 1B). This cluster harboured proteins such as G3BP, G3BP2, HuR/ELAVL1, IQGAP1, nucleolin, mTOR, RICTOR, RNA-binding protein DDX21 and some ribosomal proteins. The characteristic pattern of this cluster is the increasing ratios peaking at 60 min with a subsequent slow decrease, although proteins belonging to this cluster still maintain elevated ratios up to the 120 and 240 minutes time points. In contrast to the first three clusters that are almost exclusively composed of nuclear proteins, the fourth cluster includes several cytoplasmic proteins. Many of those proteins are also factors/members of SGs.

The fifth cluster includes proteins whose ratio peaks after 60 min with a similar pattern to the previous cluster but with a somewhat lower accumulation (Fig. 1B). Differences occur mainly at time points beyond 60 minutes as proteins in the fifth cluster display ratios close to zero or lower. This cluster can be subdivided into two distinct groups according to their profiles (Fig. 1C). The first subgroup, composed notably of ATP synthase subunits, VDACs, hexokinase, some hnRNPs and translocases, demonstrate an early elevated ratio. The second group had a delayed peak in their ratio. Proteins within this second group were almost exclusively 40S and 60S ribosomal proteins. The differences between these two groups are clearly noticeable, as seen in Fig. 1B graphs.

The last cluster contains only two proteins, NONO and SFPQ, whose abundance ratios in pADPr-binding complexes were unaffected by MNNG-induced DNA damage (Fig. 1B). Indeed, no matter what time point of MNNG incubation, SILAC ratios for these two proteins were all under 1 fold. Actually, their association ratios decrease as the MNNG time incubation increases. However, NONO and SFPQ were still immunoprecipitated in all conditions.

These distinct clusters reveal proteins with similar behaviour in relation with pADPr-association profiles. As expected, the first three clusters are composed of proteins involved in genome maintenance and integrity in response to the fast activation of PARPs and the dramatic increase in pADPr levels following genotoxic insult. In contrast, clusters four and five recruit a large number of proteins involved in cellular stress response, including mitochondrial proteins and several proteins involved in mRNA metabolism.

Western blots with antibodies against pADPr and other ligands were performed in order to validate the quantitative proteomics results. The pADPr accumulation pattern was first validated for all the time-points following PARP activation. Fig. 2A shows accumulation of pADPr in HeLa cells after 5 min of MNNG exposure. Notably, pADPr can be detected over a wide range of molecular weights. As cells are allowed to recover from MNNG treatment, the pADPr is hydrolysed by PARG so its abundance gradually decreased over time. Two hours post MNNG exposure, automodified PARP-1 can still be detected. However, after 4 hours (240 min), pADPr is almost undetectable similar to that seen at the 0 time point. This is consistent with the SILAC results as majority of proteins have ratio close to zero by 240 min. Fig. 2B validates the accumulation profiles of some proteins identified in Fig. 1.

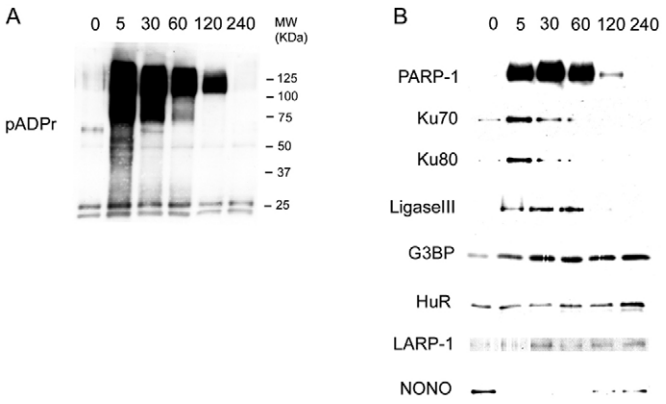

Fig. 2. Western blots used as validation tool for SILAC experiments. Cells were treated with MNNG for 5, 30 or 60 min followed by a recovery period until the 120- and 240-min time points, then analysed. (**A**) Time-course western blot analysis of pADPr accumulation in HeLa cells following MNNG treatment. pADPr-immunoprecipitated proteins were loaded and subjected to SDS-PAGE and immunoblotting against pADPr, as described in Materials and Methods. (**B**) Western blot analyses were performed on selected pADPr-binding proteins detected by MS experiments. Only molecular weight regions of the blots for the targeted proteins are shown.

These proteins are representative of the different profiles underscored by protein cluster analysis. PARP-1, DNA Ligase III, G3BP, NONO, HuR, LARP-1, Ku70 and Ku80 were assessed by western blot using specific antibodies. As shown in the proteomics profiles, proteins of the first three clusters (PARP-1, Ku70, Ku80, DNA ligase III) were detected within the first hour post-MNNG exposure, while proteins of the last three clusters (G3BP, HuR and LARP-1) were associated at later time points. Finally, NONO shows an opposite pattern with a relatively high abundance in untreated control cells, suggesting a stable association in pADPr-containing complexes in unstimulated cells.

G3BP interaction network

One of the main goals of this study was to explore the pADPr-associated proteome at the later stages of the response to DNA damage. Since the majority of the proteins identified in the third cluster belong to a group of proteins involved in the stress response (see Fig. 1A), we focused our attention on one of them, G3BP, because this protein is a major component of SGs. The immunoprecipitation of endogenous G3BP was performed under the same conditions used for the pADPr immunoprecipitations (60 min post MNNG exposure, see Fig. 1A), and G3BP-interacting proteins were identified by MS analysis. Known interactors of G3BP such as USP10, ataxin-2-like, HuR and Caprin-1 were identified with high confidence. In addition, several other G3BP-associated factors were identified, including 40S ribosomal proteins, hnRNPs, RNA helicases, LARP-1, NONO, SFPQ and PARP-1 itself (supplementary material Table S2, scaffold proteins information extracted). Interestingly, we also identified an SG-associated PARP (PARP-13) in G3BP multiprotein complexes. An overlap exists between the G3BP-interacting proteins and the pADPr interactome after 60 min of MNNG release, suggesting a connection between pADPr and G3BP interaction networks. A western blot with antibodies against pADPr clearly confirmed its accumulation in G3BP immunoprecipitates at the peak of pADPr synthesis (Fig. 3A).

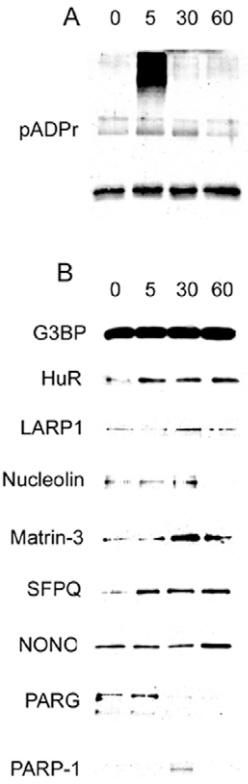

Fig. 3. pADPr is trapped in G3BP protein complexes. HeLa cells were treated with MNNG for the indicated time periods and then collected for immunoprecipitation with G3BP antibody. (**A**) Time-course western blot revealed with an antibody directed against pADPr (96-10) on G3BP immunoprecipitates. (**B**) Western blot analysis of selected proteins in G3BP immunoprecipitation extracts. Only molecular weight regions of the blots for the targeted proteins are shown.

In order to further investigate G3BP interaction network, western blots were performed on G3BP immunoprecipitates of cells that had been incubated with MNNG (Fig. 3B). Interacting partners such as NONO, SFPQ, LARP-1, HuR, Nucleolin and Matrin-3 associated with G3BP only at later time points (between 30 to 60 min) after MNNG treatment. However, the association of G3BP with PARG and pADPr (using 96-10 antibody) occurred much earlier (between 0 and 5 min post-treatment). This peak of pADPr is likely due to automodified PARP-1 even though this enzyme seems to interacts with G3BP only 30 min after MNNG treatment. Indeed, highly automodified PARP-1 gave a weaker signal than unmodified PARP. Given the already weak signal of PARP-1 at 30 min, it is probable that automodified PARP-1 is present at 5 min.

G3BP binds pADPr through its glycine-arginine-rich domain

Because large scale proteomics experiments cannot distinguish direct from indirect associations, we investigated whether G3BP binds to pADPr by transfecting cells with DNA coding for GFP-labelled G3BP or GFP alone (Fig. 4A). Immunoprecipitations were performed on both transfected cell lines (GFP-G3BP and GFP) with an antibody against GFP. On western blots of the immunoprecipitates, a band at 116 kDa representing the GFP-G3BP fusion protein was detected by both anti-GFP and anti-G3BP antibodies confirming that the fusion protein was present in the immunoprecipitates, as expected. We also observed signal at 66 kDa representing endogenous G3BP, as this protein can form homodimers and was probably associated with GFP-G3BP during the immunoprecipitation. Western blots of the immunoprecipitates using the anti-pADPr antibody, 96-10, revealed a band at 116 kDa, demonstrating the co-migration of the pADPr signal with the GFP-G3BP protein on the non-denaturing gel. In contrast, no signal was detected using anti-pADPr antibodies when cells were transfected with GFP alone. Furthermore, ^{32}P-labelled pADPr bound to both GFP-G3BP and endogenous G3BP in blots of immunoprecipitates from GFP–G3BP-transfected cells but did not bind to blots of immunoprecipitates from GFP-transfected cells. These results altogether demonstrate that G3BP binds directly pADPr *in vitro*. This is supported by previous *in vivo* results, as pADPr was shown co-migrated with G3BP in endogenous G3BP immunoprecipitation within HeLa cell line (Fig. 3B).

To determine which residues of G3BP mediate pADPr binding, we performed a pADPr dot-blot analysis with an overlapping peptide array (20-mer peptides) covering the residues of human G3BP except for the glutamate-rich region, which is very unlikely to bind a polymer with a high negative charge density. We selected an offset number of five (15 amino acids overlap) to break the G3BP peptide sequence in large overlapping fragments that are more likely to cover a pADPr-binding motif, while limiting the number of sequences to be tested (61 peptides) (Fig. 4D). The cellulose membrane containing the peptide array was incubated with radiolabelled and protein-free pADPr, washed, and exposed onto an X-ray film (Fig. 4B) and syproRuby (Fig. 4C). A radioactive pADPr signal was detected within a stretch of overlapping amino acids that cover the C-terminal glycine-rich domain of G3BP. This region of G3BP displays the properties of a bona fide pADPr-binding motif. This region is glycine-rich and extremely basic due to the presence of several arginine residues. Glycine–arginine-rich (GAR) motifs are common to several RNA-binding proteins. Studies from several laboratories have shown that lysine and arginine residues are critical for efficient recognition of the negatively charged pADPr (Malik et al., 1983; Pleschke et al., 2000; Gagné et al., 2008).

Formation of GFP-G3BP foci induced by DNA damage is pADPr-dependent and colocalizes with key proteins involved in SG formation

G3BP resides in large ribonucleoprotein complexes and initiates the formation of discrete cytoplasmic foci known as SGs. Therefore, we monitored the dynamics of G3BP-mediated SG assembly in the context of PARPs activation with MNNG. Confocal microscopy experiments were conducted both on live cells and on formaldehyde-fixed cells. The transient overexpression of G3BP results in the formation of granules, even in the absence of cellular stress. For this reason, we selected cells with modest G3BP expression. A cytoplasmic distribution of G3BP without initial aggregation was considered as the reference condition. Live cell imaging showed that, following DNA damage, GFP-G3BP aggregates in a pADPr-dependent manner. Indeed, HeLa cells exposed to MNNG begin to form G3BP foci after 15 min (Fig. 5). Pre-incubation with the PARP-1 inhibitor, ABT-888, prevented the formation of MNNG-induced stress granule assembly, implying that pADPr mediates this process. Laser-induced DNA damage targeted specifically to the cell nucleus gave similar results. The assembly of SGs triggered by the

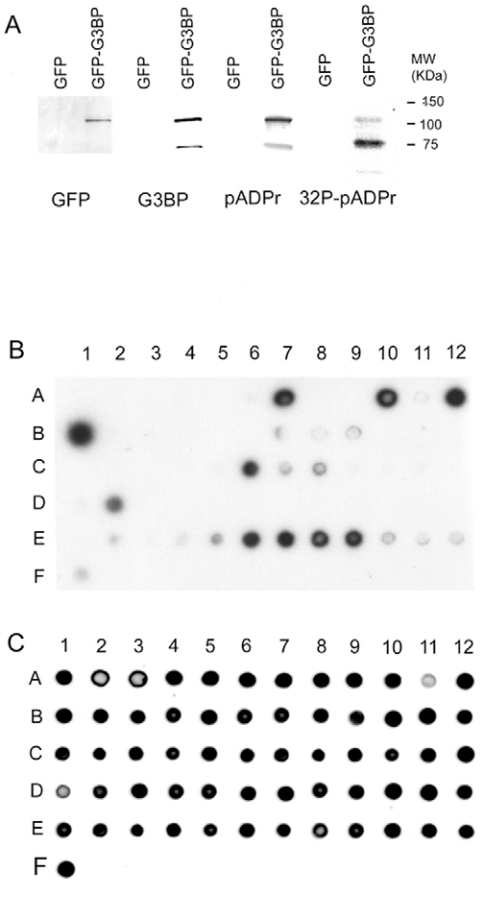

Fig. 4. G3BP binds pADPr through its glycine-arginine-rich (GAR) domain. (**A**) Western blots against GFP, G3BP and pADPr (96-10) were performed on GFP and GFP-G3BP immunoprecipitation extracts, confirming the ability of G3BP to bind pADPr. The right-hand lane shows GFP and GFP-G3BP immunoprecipitation eluates on a membrane that were incubated with ^{32}P-labelled pADPr. The expected molecular mass of G3BP is 66 kDa and that of GFP-G3BP is 116 kDa. (**B**) Determination of the pADPr-binding site of G3BP by a peptide array screening. Membrane-bound G3BP peptides (with pADPr-binding potential) were blotted with ^{32}P-labelled pADPr. Stringent conditions were applied to eliminate non-specific binding (see text). (**C**) Thereafter peptides were incubated with Sypro Ruby in order to demonstrate the integrity and event distribution of the peptides. (**D**) Membrane position and amino acids sequences of the peptide covering G3BP sequences. Several peptides were not synthesised and tested (N/S) because they were predicted to lack any pADPr-binding potential (see text).

micro-irradiation of a sub-nuclear region was also delayed by pre-incubation with PARP inhibitors. Multiple PARPs inhibitors [3AB (Durkacz et al., 1980), PJ-34 (Scott et al., 2004) and AG14361 (Veuger et al., 2003)] were tested and gave similar results (data not shown). In addition, HeLa cells exposed to H_2O_2 (1 mM) had delayed G3BP-mediated SG formation upon PARP inhibition with ABT-888 (supplementary material Fig. S1). Together, these results indicate that assembly of G3BP-containing stress granules is pADPr-dependent and that nuclear pADPr synthesis can promote the formation of cytoplasmic SGs.

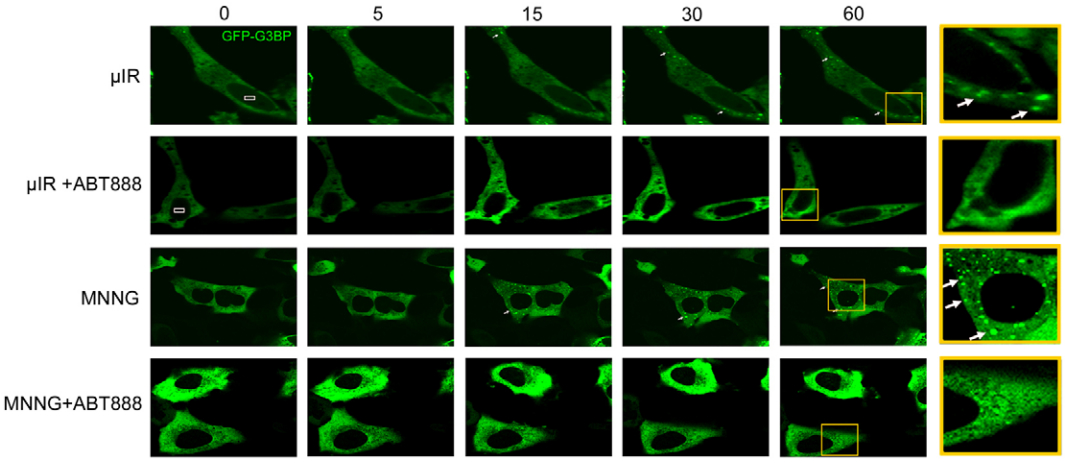

Fig. 5. Microscopy experiments with live cells reveal formation of G3BP foci upon DNA damage. A 750-nm titanium-sapphire laser was used for the micro-irradiation experiments to target a portion of the nucleus thereby inducing DNA damage in HeLa cells. The laser track is represented as a white box. Micro-irradiated experiments (μIR) demonstrated formation of GFP-G3BP foci within 15 min. Formation of GFP-G3BP was delayed in cells treated with 5 μM PARP inhibitors (ABT-888). In addition, MNNG treatment (MNNG) also induced GFP-G3BP foci within 15 min. Addition of ABT-888 1 hour prior to MNNG incubation delayed formation of GFP-G3BP foci. White arrows indicate G3BP-containing SGs. Images on the far right are higher magnifications of boxed areas.

SG assembly not only involves G3BP but also several other proteins. Confocal microscopy was performed on endogenous markers of SGs to further validate that the large cytoplasmic G3BP-containing subcellular structures that we observed upon MNNG exposure were actually SGs. Cells were incubated with MNNG for 30 min, fixed and analysed for the formation of SG (Fig. 6). The SG markers eIF4E (Kedersha et al., 2005), TIAR (Kedersha et al., 2005) and HuR (Kedersha and Anderson, 2002) were detected by microscopy to determine whether they colocalized with GFP-G3BP. Indeed, we observed that GFP-G3BP colocalized with all these factors. Interestingly, we observed that LARP-1, which has been shown to associate with P bodies in *C. elegans* (Nykamp et al., 2008), also colocalizes with GFP-G3BP in SGs induced by genotoxic stress. In fact, a proportion of the LARP-1 in the cell colocalized with GFP-G3BP, while the rest aggregated in foci within the cytoplasm suggesting a probable distribution of LARP-1 in mammalian SGs.

GFP-G3BP subcellular localisation is affected by pADPr but not by Leptomycin B

One important G3BP feature revealed by the present study is the identification of a pADPr-binding site in the GAR domain of G3BP. Several RNA-associated proteins contain a GAR domain, including the SR family proteins that shuttle between the nucleus and cytoplasm (reviewed by Godin and Varani, 2007). Because the arginine-rich domains have been implicated in nucleocytoplasmic shuttling, we investigated the possible modulation of this phenomenon by poly(ADP-ribosyl)ation. HeLa cells were co-transfected with GFP-G3BP- and mCherry-PARG-expressing vectors in order to modulate pADPr levels (Fig. 7). When GFP-G3BP was co-transfected with the wild-type 111-kDa PARG (PARG111WT) nuclear isoform, we observed a significant accumulation of GFP-G3BP in the nucleus, indicating a disruption of the nuclear export of G3BP. In contrast, the co-expression of a dominant negative 111-kDa PARG mutant (PARG111DEAD) did not affect the subcellular localisation of GFP-G3BP which remained cytoplasmic. This result suggests that the presence of pADPr can regulate the nucleocytoplasmic movement of G3BP. This cellular movement of G3BP seems to be important for the assembly of SGs since no G3BP-containing granules were observed in PARG111WT-expressing cells in contrast to cell expressing PARG111DEAD. This was further investigated by treating the cells with Leptomycin B (LMB), a potent and specific CRM1-dependent inhibitor of nuclear export (Gallouzi et al., 2001). HeLa cells were incubated with 10 ng/ml LMB for 20 hours prior to live cell imaging. LMB induced no subcellular variation as GFP-G3BP remained cytoplasmic and foci were observed upon cellular damage (Fig. 8). Together these results suggest that CRM1 nuclear export pathway does not appear to be involved in G3BP nucleocytoplasmic shuttling, while pADPr seems to act as a modulator of G3BP nuclear export.

Discussion

In this study, we present the first dynamic overview of the pADPr-associated proteome following MNNG-induced DNA damage. Large-scale quantitative mass spectrometry based on SILAC technology (Ong et al., 2002) constituted the first phase of an investigation undertaken to better understand the cellular response to DNA damage and PARP activation beyond the initial DNA-damaging and recognition events. A protein clustering based on their enrichment ratios in pADPr immunoprecipitates at different time points following PARPs activation was used to separate proteins into functionally related groups. As expected, DNA damage signalling and repair proteins are clustered into early clusters that associate with pADPr upon PARPs activation. This is consistent with the current model where pADPr is viewed as a loading platform for the recruitment and assembly of

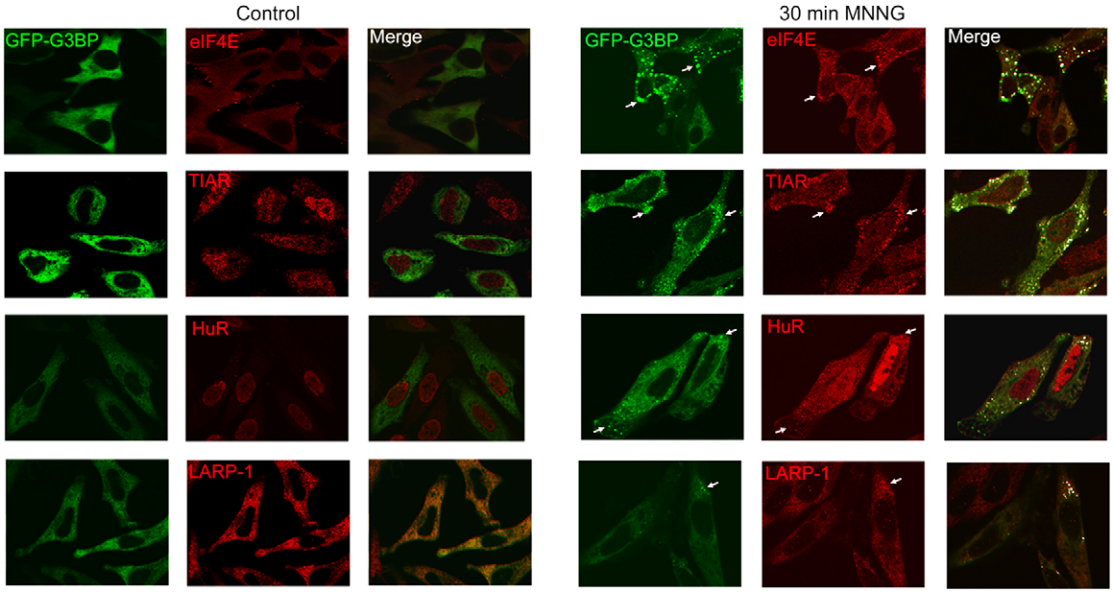

Fig. 6. G3BP colocalizes with key proteins after genotoxic stress induced by MNNG. DNA coding for GFP-G3BP was transfected in HeLa cells then cells were fixed and stained with selected antibodies. Alexa Fluor 564 secondary antibodies were used to detect the primary antibodies. Proteins other than GFP-G3BP are represented in the red channel. Colocalization was investigated in unstressed (control) and in stress-induced cells (30 min MNNG). ImageJ was used to identify colocalization patterns that are represented in white. White arrows indicate G3BP-containing SGs.

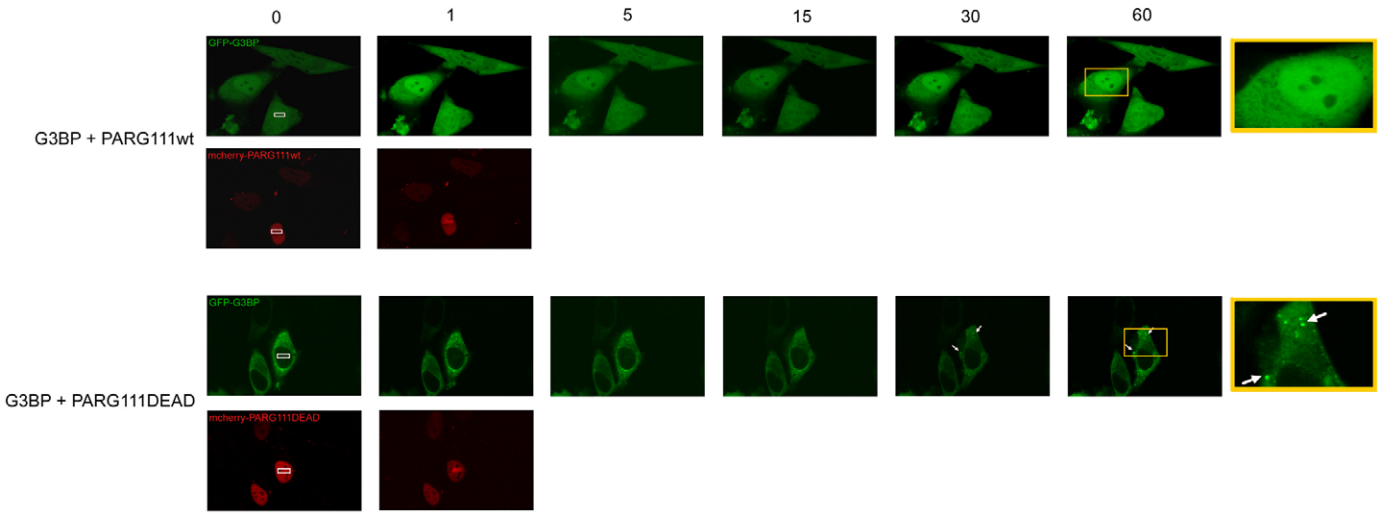

Fig. 7. Co-transfection of DNA coding for GFP-G3BP and PARG111 suggests a role for pADPr in the nucleocytoplasmic movement of G3BP. A titanium-sapphire laser was used to create DNA damage within a region of the nucleus in HeLa cells. The laser track is represented as white box. Co-transfection of DNA coding for mCherryPARG$_{111wt}$ with GFP-G3BP induces both nuclear and cytoplasmic localisation of GFP-G3BP. However, formation of GFP-G3BP foci is blocked, and mCherryPARG$_{111wt}$ is recruited to the laser track. On the other hand, co-transfection of DNA coding for mCherryPARG$_{111DEAD}$ and GFP-G3BP induced no change in GFP-G3BP localisation; GFP-G3BP is exclusively cytoplasmic. Micro-irradiation induces GFP-G3BP foci, and mCherryPARG$_{111DEAD}$ was recruited and accumulated at the laser track. White arrows indicate G3BP-containing SGs. Images on the far right are higher magnifications of boxed areas.

multiprotein repair complexes. However, this study took advantage of high-throughput mass spectrometry analysis to analyse pADPr-associated complexes at later time points, up to 4 hours post MNNG exposure. It has been known for a long time that pADPr levels are transient and spontaneously resolving after rapid degradation by PARG. However, there is an apparent gap between our understanding of the initial pADPr-associated molecular events underlying DNA damage, major nuclear reorganization and cytoplasmic events, and the profound impact of pADPr on cell fate. Our study uncovers novel complexes interacting with pADPr in phases subsequent to recruitment of DNA damage response protein induced by genotoxic stress, shedding light on the pADPr mechanistic. The quantitative proteomics results represent evidence of temporal clustering of pADPr-associated proteins in distinct biological processes following MNNG-induced DNA damage. These clusters of proteins suggest a temporal mechanism of pADPr regulation for cell fate. Indeed, it first associates with DNA damage response proteins then pADPr association is shifted towards mRNA maturation proteins (several found with nucleocytoplasmic shuttling abilities), ribosomal proteins and several mitochondrial proteins.

We present the first evidence that pADPr is involved in the assembly of SGs. Indeed, several proteins involved in SG formation accumulate at later time points in pADPr-containing complexes. Investigation of interplay between pADPr and SGs was focused through analysis of the involvement of G3BP1. We showed that alkylation-induced DNA damage results in the formation of G3BP1-containing SGs in a pADPr-dependent fashion. Other DNA damaging agents such as H_2O_2 or UV irradiation are known to induce SG assembly and PARPs activation (Anderson and Kedersha, 2002; Kimball et al., 2003). However, we demonstrate for the first time a stress-specific function of the pADPr in the assembly of SGs. This finding gives us a better understanding of the link between DNA damage response and the formation of SGs. A recent study from Leung and colleagues reported that pADPr modulates the assembly and maintenance of cytoplasmic SGs and that specific PARPs and PARG isoforms associate with cytoplasmic mRNP complexes (Leung et al., 2011). Although we do not exclude a role for cytoplasmic SG-PARPs in pADPr-mediated stress response, our results suggest that the DNA-dependent PARPs (PARP-1 and PARP-2) are major modulators of cytoplasmic SG formation through pADPr synthesis. Actually, we also identified the SG-associated PARP-13 in a cluster of proteins that includes several SG components, and we were the first group to characterise the localisation of PARG into cytoplasmic mRNPs (Gagné et al., 2005). This present study

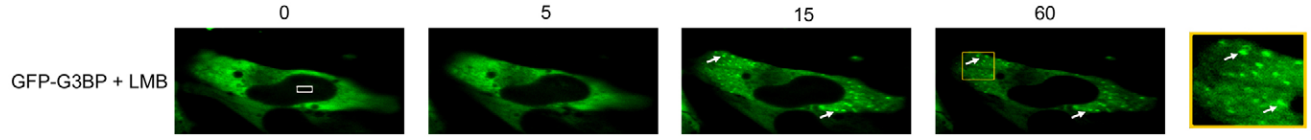

Fig. 8. Live cell microscopy reveals that formation of G3BP foci upon DNA damage is unaffected by Leptomycin B. HeLa cells were incubated for 29 hours with 10 ng/ml LMB prior to the micro-irradiation experiments. The laser track (represented as a white box) targeted a portion of the nucleus thereby inducing DNA damage. Mirco-irradiation experiments induced GFP-G3BP foci, even with earlier LMB treatment. White arrows indicate G3BP-containing SGs. Images on the far right are higher magnifications of boxed areas.

was performed in the context of strong PARP-1/2 activation with a DNA alkylating agent, while the study of Leung et al. employed sodium arsenite to induce SG formation (Leung et al., 2011). Ding et al. report that arsenite inhibits oxidative DNA damage repair and suggests that interaction of arsenite with the PARP-1 zinc finger domain contributes to the inhibition of PARP-1 activity by arsenite (Ding et al., 2009). However, PARP-2, which do not possesses zinc-finger structures, would still be strongly activated by arsenite exposure through the generation of reactive oxygen species associated with DNA damage. While both MNNG and arsenite trigger DNA damage and PARP activation, these chemicals can also exhibit non-specific adverse effects in cells. In order to ascertain that nuclear poly(ADP-ribosyl)ation is involved in the assembly of cytoplasmic SGs, laser-induced DNA damage was generated in a limited sub-nuclear region of the cell by two-photon confocal microscopy. The results thus obtained reveal same the pADPr-dependent mechanism as with the results acquired by MNNG-stressed cells.

Investigation of interplay between pADPr and SGs was focused through analysis of the role of G3BP. A key function of SG formation is to concentrate certain cellular components in the granules, while reducing their concentration in the rest of the cytosol. This feature may serve pADPr in two ways. One possibility is that pADPr alters the activities and interactions of proteins in the SG. In fact, pADPr is already known to interfere with domain essential to protein-protein interaction and has the ability to act as a scaffold molecule. For example, pADPr will most likely modulate activities of proteins within SGs, as seen with the ability of pADPr to shift activity of topoisomerase I towards ASF/SF2 (Yung et al., 2004; Malanga et al., 2008) or the postulated ability of pADPr to modulate the activity of hnRNPs, thereby affecting mRNA splicing (Ji and Tulin, 2009). Moreover, Leung et al. demonstrate that pADPr modulates the assembly and maintenance of an mRNP-enriched structure. Indeed, a possible function of SGs is to stabilise mRNA (Leung et al., 2011). Protein aggregation in SG increases concentration of molecules locally which supports a higher rate of biochemical reaction and protein contact density. This is consistent with our hypothesis that views pADPr as a SG and G3BP regulator. Mapping of G3BP pADPr-binding indicates that the C-terminal glycine- and arginine-rich (GAR) region is a non-covalent pADPr-binding domain. The identification of a similar pADPr-binding GAR in the mRNA-binding protein ASF/SF2 supports our identification of the GAR region of G3BP as the pADPr-binding region (Malanga et al., 2008). Several reports indicate that GAR coordinates mRNA maturation events and mediates the nucleocytoplasmic trafficking of numerous RNA-binding proteins (reviewed by Godin and Varani, 2007). Clearly, our results indicate that nuclear export of G3BP is deregulated when PARG is overexpressed. PARG overexpression directly impacts, by reducing its half-life time, the cellular pADPr levels no matter which isoform of PARG is expressed (nuclear or cytoplasmic) since all PARG isoforms constantly shuttle between the nucleus and cytoplasm (Haince et al., 2006; Mortusewicz et al., 2011). Moreover, Tourrière et al. demonstrated that a G3BP C-terminal deletion (which encompass GAR region) considerably reduces SG formation efficiency (Tourrière et al., 2003). The hypothesis of pADPr regulating SG formation is supported by similar role of pADPr in the nucleus. Indeed, Tulin and co-workers discovered that PARP1 automodification is required for shuttling key proteins into Cajal bodies by protein non-covalent interaction with pADPr *in vivo* (Kotova et al., 2009).

SGs may also act as refuge for pADPr as PARG activities in the cytoplasm are higher than in the nucleus. SG formation plays a role during the stress response in cell fate decisions. Actually, SGs harbour several apoptosis regulatory actors and provide a protective role during stress as impairing SG assembly often leads to poorer cell survival rate (Baguette et al., 2007). Therefore, SGs sheltering of pADPr could prevent AIF release, while preserving and accumulating pADPr in the cytoplasm until cellular mechanisms reaching a critical point in which the cell fate is directed toward pADPr-dependent apoptosis (Andrabi et al., 2008; David et al., 2009). As long and branched pADPr is more likely to cause AIF release (Andrabi et al., 2006; Yu et al., 2006), this type of molecule is unlikely to leave the nucleus intact as most of it attached to PARP-1 [and PARP-2 (automodification)]. There is, however, a possible hypothesis for pADPr association with SGs. Indeed, the biphasic PARG activity (Brochu et al., 1994) has higher affinity for long and branched pADPr, subsequently releasing shorter molecule free into the nucleoplasm with higher half-life than the long and complex pADPr (Alvarez-Gonzalez and Althaus, 1989). Therefore, the necessity of amassing greater quantity of shorter pADPr to induce parthanatos could be an SG function upon genotoxic stress. Indeed, G3BP immunoprecipitation results suggest a higher level of interaction after longer genotoxic stress. In addition, Kromer and colleagues demonstrate AIF functions as an endogenous repressor of cytoplasmic SG formation and also show dissociation of the pro-apoptotic and the anti-SG activities of AIF (Candé et al., 2004). Therefore, SGs could be a critical structure in the crosstalk between apoptosis and stress response.

Previous studies have shown that PARPs are rapidly relocated to sites of DNA damage resulting in the dramatic increase of pADPr levels in the vicinity of the lesion (Dantzer et al., 2006; Haince et al., 2008). In this study, we showed that pADPr migration into a microirradiated nuclear area is sufficient to induce cytoplasmic SG formation and that PARP inhibition abrogates the assembly of SGs under the same conditions. Although, the mechanism by which pADPr translocates from the nucleus to the cytoplasm is unknown our results suggest that this translocation is essential for the orchestration of the SG assembly, in addition to a fundamental process involved in parthanatos cell death (Wang et al., 2011).

In view of these findings implicating pADPr in the regulation of cellular stress response, we hypothesise that pADPr could act as a nucleation or aggregation site for the assembly of SGs. Alternatively, pADPr may be trapped in SGs and protected from PARG degradation in the cytoplasm. SGs harbour several apoptosis regulatory factors and provide a protective role during stress since impairing SG assembly often leads to poorer cell survival rate (Baguet et al., 2007). Therefore, sheltering pADPr in SGs could prevent mitochondrial disfunction to a certain extent until a critical point where extensive stress would trigger pADPr-dependent cell death. Our exploratory study of the pADPr-associated proteins dynamics indicates that pADPr is a critical effector of the cellular response to stress through modulation of SG assembly. This study describes for the first-time the late pADPr interaction network along with evidence that pADPr is the effector molecule underlying SG assembly upon genotoxic insult.

Materials and Methods

Cell culture and expression vectors

HeLa cells were cultured (5% CO_2, 37℃) in DMEM supplemented with 10% fetal bovine serum (Hyclone-ThermoFisher Scientific). Penicillin (100 U/ml) and streptomycin (100 mg/ml) (Wisent, Canada) were added to culture media. For SILAC experiments, cells were grown in culture media with Arg and Lys amino acids containing naturally occurring atoms (referred as the light culture) or their stable isotope counterparts [$^{13}C_6$]lysine and [$^{13}C_6{}^{15}N_4$]arginine (Cambridge Isotope Labs) for at least five divisions to allow for full incorporation of labelled amino acids. Six dishes of 15 cm were used per condition (~40 millions HeLa cells). Experiments were performed in triplicate.

The GFP-G3BP expression vector was a gift from Dr Jamal Tazi (Institut de Génétique Moléculaire de Montpellier). The full-length cDNA corresponding to G3BP was fused in frame to the GFP by inserting a *Bgl*II-*Eco*RI fragment into pEGFP-C1 vector as described previously (Tourrière et al., 2001). The mCherry-PARG expression vectors were prepared by transferring the PARG coding sequence of the GFP-hPARG-110 (pEGFP-C1, Clontech) described previously (Haince et al., 2006) into pmCherry-C1 (Clontech). These expression plasmids encode the full-length wild-type human PARG 111 kDa nuclear isoform (mCherry-PARG-WT) and a dominant-negative version of the construct (mCherry-PARG-DEAD). The mCherry-PARG-DEAD-expressing vector was prepared by oligonucleotide-directed mutagenesis. Mutagenic primers were made following the guidelines in the QuikChange® site-directed mutagenesis kit (Stratagene). A mutation was introduced at amino acid position 756 that completely abolish PARG catalytic activity (E756D) as reported previously (Patel et al., 2005; Haince et al., 2006). Transfections were carried out with Effectene transfection reagent (Qiagen) as recommended by the manufacturer and cells were analysed 24 hours post-transfection.

Dynamic imaging and immunofluorescence microscopy

Localised laser micro-irradiation of subnuclear regions was performed essentially as described previously (Haince et al., 2008). Briefly, HeLa cells were seeded onto 35 mm glass bottom dishes (MatTEK Corporation), transfected overnight with GFP-G3BP and sensitised in medium containing 1 μg/ml Hoescht 33342 (Sigma) for 30 min. A 37℃ preheated stage with continuous 5% CO_2 perfusion was used for the time-lapse imaging on a Zeiss LSM 510 META NLO laser-scanning confocal microscope. The acquisition rate was every 5 min over 120 min (Haince et al., 2008).

For immunofluorescence experiments, cells were fixed after N-methyl-N′-nitro-N-nitrosoguanidine (MNNG) exposure at the indicated time-points with 4% formaldehyde in phosphate-buffered saline (pH 7.5) for 15 min at room temperature. Cells were immunostained with combinations of antibody (specified in the Fig. 7 legend) for 2 hours subsequent to permeabilisation with Triton X-100 solution in PBS. Cells were washed twice with phosphate-buffered saline prior a to 30-minutes incubation with an appropriate secondary antibody conjugated to Alexa Fluor 541. Finally, formaldehyde-fixed cells were counterstained with Hoechst 1 μg/ml 33258 for 5 min to stain DNA. A Zeiss LSM 510 laser-scanning confocal microscope was used for image acquisition. Colocalizations were performed using ImageJ 1.44 (NIH) software with Colocalization plugin. This plugin highlights the colocalized points of two 8-bit images (or stacks). The colocalized points will appear white by default (display value=255). Two points are considered as colocalized if their respective intensities are strictly higher than the threshold of their channels (threshold channel: 50), and if their ratio (of intensity) is strictly higher than the ratio setting value (ratio: 50%). Composite figures of collected images were assembled in Adobe Photoshop. Experiments were repeated at least 10 times for both dynamic imaging and immunofluorescence microscopy analyses.

Peptide polymer blot analysis

The 466 amino acids sequence of G3BP (Uniprot accession code Q13283) was used to generate an overlapping peptide library. The library is composed of 20-mer peptides with 5 amino acid off-set (91 peptides). Peptides were synthesised on cellulose membrane by SPOT technology using an automated multiple synthesiser (MultiPep RS, Intavis) as described previously (Smith et al., 2011). The membrane was rinsed with a small volume of methanol for 5 min to avoid precipitation of hydrophobic peptides during the subsequent TBS washing procedure. The membrane was incubated for 1 h at room temperature with gentle agitation in TBS-T (10 mM Tris-HCl pH 8.0, 150 mM NaCl, 0.1% Tween-20) containing 250 nM of DHBB-purified ^{32}P-labelled pADPr synthesised as described previously (Gagné et al., 2008). The membrane was washed several times with TBS-T until no radioactivity could be detected in the washes. Subsequently, the membrane was air-dried and subjected to autoradiography. Sypro Ruby (BioRad) staining was applied after autoradiography in order to verify peptide synthesis. Staining was performed according to the manufacturer's instructions.

Immunoprecipitation and immunoblotting

HeLa cells were grown at 80–90% confluence in 150 mm culture dishes. MNNG treatment (100 μM) was performed for each time point (5, 30, 60, 120 and 240 minutes) then cells were washed with ice-cold phosphate-buffered saline (PBS). Ice-cold phosphate lysis buffer (40 mM HEPES pH 7.5, 120 mM NaCl, 0.3% CHAPS, 1 mM EDTA, 1 μM ADP-HPD (PARG inhibitor, Calbiochem) and 1× complete protease inhibitor cocktail (Roche Applied Science) was added to cells. Cells were harvested using a cell scraper. Lysed cells collected from six dishes were pooled, then gently mixed by inversion for 1 hour at 4℃ on a rotating device, and centrifuged for 10 min at 6000 ***g*** to remove insoluble cellular debris. The cellular extract was mixed with magnetic beads coupled to protein G (Invitrogen) and the appropriate antibody against pADPr (mouse monoclonal clone 10H, Tulip Biolabs), or G3BP (mouse monoclonal, BD Biosciences) or anti-GFP (mouse monoclonal Roche), or normal mouse IgG for the control, and incubated 2 hours at 4℃ with rotation. For all pull-down conditions, beads were previously blocked for 1 hour with 1% BSA in PBS and washed with the appropriate lysis buffer before specific antibody coupling. Proteins were eluted from the beads by boiling for 5 min in Laemmli SDS sample buffer containing 5% (v/v) β-mercaptoethanol and kept at −30℃ until further analysis.

For western blot analysis, eluted proteins extracts were resolved by SDS-PAGE and then transferred onto 0.2 μm nitrocellulose membrane (Bio-Rad, Canada). After one hour incubation with a blocking solution (PBS-T containing 5% non-fat dried milk), the membrane was probed overnight at 21℃ with shaking, with either: primary antibodies to PARP-1 (clone C2-10), X-ray repair cross-complementing protein 5 (XRCC5/Ku80) (Oncogene Research Products), X-ray repair cross-complementing protein 6 (XRCC6/Ku70) (Oncogene Research Products), G3BP (BD Bioscience), Nucleolin (Abcam), HuR (Santa Cruz Biotech), PARG (Millipore), LARP-1 (Abcam), Matrin-3 (Abcam), NONO (Bethyl Laboratories), SFPQ (Bethyl Laboratories), Ligase III (Invitrogen). After extensive washing with the blocking solution, membranes were incubated for 1 hour with species-specific horseradish peroxidase-conjugated secondary antibodies. Signals were detected with the Western Lightning Chemiluminescence reagent plus kit (Perkin Elmer).

nanoLC-MS/MS

Proteins eluted from the immunoprecipitated material were resolved using 4–12% Criterion XT Bis–Tris gradient gel (Bio-Rad, Mississauga, Canada) and stained with Sypro Ruby (Bio-Rad, Mississauga, ON) according to the manufacturer's instructions. Images were acquired using a Geliance CCD-based imaging system (Perkin-Elmer). The entire protein profile on the gel was sliced into 24 sections using a gel excision Lanepicker (The Gel Company). In-gel protein digests were performed using sequencing-grade modified trypsin (Promega). Peptide extracts were dried, reconstituted in 0.1% formic acid, and analysed by LC–MS/MS using an Agilent 1100 nanoLC system coupled to a qQTOF mass spectrometer (QSTAR XL, MDS Analytical Technologies) equipped with nanoESI source. Peptides were separated using a New Objective column running at 250 nl/min with a 45-minute linear separation gradient from 10-40% B followed by a 20-minutes linear gradient from 40% to 80% B (buffers A, 0.1% formic acid in water and B, 0.1 formic acid in acetonitrile). Mass spectra were acquired using a data-dependent acquisition mode, whereby each MS-only scan (400 to 1800 m/z) was followed by CID of the three most intense ions having a +2, +3 or +4 charge. Fragmented precursors were dynamically excluded for 60 seconds with a 100-ppm mass tolerance.

Bioinformatics and data analysis

All MS/MS spectra were analysed using Mascot (Matrix Science, version 2.2.0). Mascot was set up to search against the human International Protein Index (IPI) database (IPI version 3.87, 89,432 entries as of December 2010 with the addition of 35 protein sequences corresponding to proteins of interests such as PARP isoforms) assuming a digestion with trypsin. Fragment and parent ion mass tolerance were respectively of 0.25 Da and 0.25 Da. Iodoacetamide derivative of cysteine was specified as a fixed modification. Deamidation of asparagine and glutamine, acetylation of lysine and arginine and oxidation of methionine were specified as variable modifications. Two missed cleavages were allowed.

Scaffold (version Scaffold_3_00_05, Proteome Software Inc.) was used to validate MS/MS based peptide and protein identifications. Peptide identifications were accepted if they could be established at greater than 95.0% probability as specified by the Peptide Prophet algorithm (Keller et al., 2002). Protein identifications were accepted if they could be established at greater than 95.0% probability and contained at least two unique peptides. Protein probabilities were assigned by the Protein Prophet algorithm (Nesvizhskii et al., 2003). Proteins that contained similar peptides and could not be differentiated based on MS/MS analysis alone were grouped to satisfy the principle of parsimony.

For SILAC-based quantitation analysis, ProteinPilot4 (AB Sciex, Canada) was used to validate MS/MS based peptide and protein identifications, as well as calculating the ratios for each peptides and proteins using the 'thorough search' and 'biological modification ID focus' option. Iodoacetamide derivative of cysteine was specified as a fixed modification. Peptide and Protein with 95% and more confidence (ProtScore>1.3) were reported. Protein ratios with a *P*-value less than 0.1 and an error factor less than 2 were considered reliable. The default ion intensity threshold in ProteinPilot4 for calculating peptide ratios was 40 counts.

K-means (calculated means mode) clustering was performed based on Euclidean distance with average linkage using the MultiExperiementViewer (version 4.7.4) program (Saeed et al., 2003).

Funding

This work was supported by the Canadian Institutes of Health Research [grant numbers MO-178013 to G.G.P.; MOP-119358 and MOP-897998 to I.E.G]; Fonds de la Recherche en Sante du Quebec [grant 13971 to M.I.]. I.E.G. is a recipient of a TierII Canada Research Chair. G.G.P. holds a Canada Research Chair in Proteomics.

Supplementary material available online at
http://jcs.biologists.org/lookup/suppl/doi:10.1242/jcs.106963/-/DC1

References

Albaum, S. P., Hahne, H., Otto, A., Haußmann, U., Becher, D., Poetsch, A., Goesmann, A. and Nattkemper, T. W. (2011). A guide through the computational analysis of isotope-labeled mass spectrometry-based quantitative proteomics data: an application study. *Proteome Sci.* **9**, 30.

Alvarez-Gonzalez, R. and Althaus, F. R. (1989). Poly(ADP-ribose) catabolism in mammalian cells exposed to DNA-damaging agents. *Mutat. Res.* **218**, 67-74.

Amé, J. C., Rolli, V., Schreiber, V., Niedergang, C., Apiou, F., Decker, P., Muller, S., Höger, T., Ménissier-de Murcia, J. and de Murcia, G. (1999). PARP-2, A novel mammalian DNA damage-dependent poly(ADP-ribose) polymerase. *J. Biol. Chem.* **274**, 17860-17868.

Anderson, P. and Kedersha, N. (2002). Stressful initiations. *J. Cell Sci.* **115**, 3227-3234.

Anderson, P. and Kedersha, N. (2009). RNA granules: post-transcriptional and epigenetic modulators of gene expression. *Nat. Rev. Mol. Cell Biol.* **10**, 430-436.

Andrabi, S. A., Kim, N. S., Yu, S. W., Wang, H., Koh, D. W., Sasaki, M., Klaus, J. A., Otsuka, T., Zhang, Z., Koehler, R. C. et al. (2006). Poly(ADP-ribose) (PAR) polymer is a death signal. *Proc. Natl. Acad. Sci. USA* **103**, 18308-18313.

Andrabi, S. A., Dawson, T. M. and Dawson, V. L. (2008). Mitochondrial and nuclear cross talk in cell death: parthanatos. *Ann. N. Y. Acad. Sci.* **1147**, 233-241.

Baguet, A., Degot, S., Cougot, N., Bertrand, E., Chenard, M. P., Wendling, C., Kessler, P., Le Hir, H., Rio, M. C. and Tomasetto, C. (2007). The exon-junction-complex-component metastatic lymph node 51 functions in stress-granule assembly. *J. Cell Sci.* **120**, 2774-2784.

Brochu, G., Duchaine, C., Thibeault, L., Lagueux, J., Shah, G. M. and Poirier, G. G. (1994). Mode of action of poly(ADP-ribose) glycohydrolase. *Biochim. Biophys. Acta* **1219**, 342-350.

Candé, C., Vahsen, N., Métivier, D., Tourrière, H., Chebli, K., Garrido, C., Tazi, J. and Kroemer, G. (2004). Regulation of cytoplasmic stress granules by apoptosis-inducing factor. *J. Cell Sci.* **117**, 4461-4468.

D'Amours, D., Desnoyers, S., D'Silva, I. and Poirier, G. G. (1999). Poly(ADP-ribosyl)ation reactions in the regulation of nuclear functions. *Biochem. J.* **342**, 249-268.

Dantzer, F., Amé, J. C., Schreiber, V., Nakamura, J., Ménissier-de Murcia, J. and de Murcia, G. (2006). Poly(ADP-ribose) polymerase-1 activation during DNA damage and repair. *Methods Enzymol.* **409**, 493-510.

David, K. K., Andrabi, S. A., Dawson, T. M. and Dawson, V. L. (2009). Parthanatos, a messenger of death. *Front. Biosci.* **14**, 1116-1128.

Ding, W., Liu, W., Cooper, K. L., Qin, X. J., de Souza Bergo, P. L., Hudson, L. G. and Liu, K. J. (2009). Inhibition of poly(ADP-ribose) polymerase-1 by arsenite interferes with repair of oxidative DNA damage. *J. Biol. Chem.* **284**, 6809-6817.

Durkacz, B. W., Omidiji, O., Gray, D. A. and Shall, S. (1980). (ADP-ribose)n participates in DNA excision repair. *Nature* **283**, 593-596.

Gagné, J. P., Hunter, J. M., Labrecque, B., Chabot, B. and Poirier, G. G. (2003). A proteomic approach to the identification of heterogeneous nuclear ribonucleoproteins as a new family of poly(ADP-ribose)-binding proteins. *Biochem. J.* **371**, 331-340.

Gagné, J. P., Bonicalzi, M. E., Gagné, P., Ouellet, M. E., Hendzel, M. J. and Poirier, G. G. (2005). Poly(ADP-ribose) glycohydrolase is a component of the FMRP-associated messenger ribonucleoparticles. *Biochem. J.* **392**, 499-509.

Gagné, J. P., Isabelle, M., Lo, K. S., Bourassa, S., Hendzel, M. J., Dawson, V. L., Dawson, T. M. and Poirier, G. G. (2008). Proteome-wide identification of poly(ADP-ribose) binding proteins and poly(ADP-ribose)-associated protein complexes. *Nucleic Acids Res.* **36**, 6959-6976.

Gallouzi, I. E., Brennan, C. M. and Steitz, J. A. (2001). Protein ligands mediate the CRM1-dependent export of HuR in response to heat shock. *RNA* **7**, 1348-1361.

Godin, K. S. and Varani, G. (2007). How arginine-rich domains coordinate mRNA maturation events. *RNA Biol.* **4**, 69-75.

Haince, J. F., Ouellet, M. E., McDonald, D., Hendzel, M. J. and Poirier, G. G. (2006). Dynamic relocation of poly(ADP-ribose) glycohydrolase isoforms during radiation-induced DNA damage. *Biochim. Biophys. Acta* **1763**, 226-237.

Haince, J. F., McDonald, D., Rodrigue, A., Déry, U., Masson, J. Y., Hendzel, M. J. and Poirier, G. G. (2008). PARP1-dependent kinetics of recruitment of MRE11 and NBS1 proteins to multiple DNA damage sites. *J. Biol. Chem.* **283**, 1197-1208.

Harsha, H. C., Molina, H. and Pandey, A. (2008). Quantitative proteomics using stable isotope labeling with amino acids in cell culture. *Nat. Protoc.* **3**, 505-516.

Hassa, P. O. and Hottiger, M. O. (2008). The diverse biological roles of mammalian PARPS, a small but powerful family of poly-ADP-ribose polymerases. *Front. Biosci.* **13**, 3046-3082.

Iliuk, A., Galan, J. and Tao, W. A. (2009). Playing tag with quantitative proteomics. *Anal. Bioanal. Chem.* **393**, 503-513.

Ji, Y. and Tulin, A. V. (2009). Poly(ADP-ribosyl)ation of heterogeneous nuclear ribonucleoproteins modulates splicing. *Nucleic Acids Res.* **37**, 3501-3513.

Kedersha, N. and Anderson, P. (2002). Stress granules: sites of mRNA triage that regulate mRNA stability and translatability. *Biochem. Soc. Trans.* **30**, 963-969.

Kedersha, N., Stoecklin, G., Ayodele, M., Yacono, P., Lykke-Andersen, J., Fritzler, M. J., Scheuner, D., Kaufman, R. J., Golan, D. E. and Anderson, P. (2005). Stress granules and processing bodies are dynamically linked sites of mRNP remodeling. *J. Cell Biol.* **169**, 871-884.

Keller, A., Nesvizhskii, A. I., Kolker, E. and Aebersold, R. (2002). Empirical statistical model to estimate the accuracy of peptide identifications made by MS/MS and database search. *Anal. Chem.* **74**, 5383-5392.

Kim, M. Y., Zhang, T. and Kraus, W. L. (2005). Poly(ADP-ribosyl)ation by PARP-1: 'PAR-laying' NAD+ into a nuclear signal. *Genes Dev.* **19**, 1951-1967.

Kimball, S. R., Horetsky, R. L., Ron, D., Jefferson, L. S. and Harding, H. P. (2003). Mammalian stress granules represent sites of accumulation of stalled translation initiation complexes. *Am. J. Physiol. Cell Physiol.* **284**, C273-C284.

Kotova, E., Jarnik, M. and Tulin, A. V. (2009). Poly (ADP-ribose) polymerase 1 is required for protein localization to Cajal body. *PLoS Genet.* **5**, e1000387.

Leung, A. K., Vyas, S., Rood, J. E., Bhutkar, A., Sharp, P. A. and Chang, P. (2011). Poly(ADP-ribose) regulates stress responses and microRNA activity in the cytoplasm. *Mol. Cell* **42**, 489-499.

Lindahl, T., Satoh, M. S., Poirier, G. G. and Klungland, A. (1995). Post-translational modification of poly(ADP-ribose) polymerase induced by DNA strand breaks. *Trends Biochem. Sci.* **20**, 405-411.

Malanga, M., Czubaty, A., Girstun, A., Staron, K. and Althaus, F. R. (2008). Poly(ADP-ribose) binds to the splicing factor ASF/SF2 and regulates its phosphorylation by DNA topoisomerase I. *J. Biol. Chem.* **283**, 19991-19998.

Malik, N., Miwa, M., Sugimura, T., Thraves, P. and Smulson, M. (1983). Immunoaffinity fractionation of the poly(ADP-ribosyl)ated domains of chromatin. *Proc. Natl. Acad. Sci. USA* **80**, 2554-2558.

Montes de Oca, R., Shoemaker, C. J., Gucek, M., Cole, R. N. and Wilson, K. L. (2009). Barrier-to-autointegration factor proteome reveals chromatin-regulatory partners. *PLoS ONE* **4**, e7050.

Mortusewicz, O., Fouquerel, E., Amé, J. C., Leonhardt, H. and Schreiber, V. (2011). PARG is recruited to DNA damage sites through poly(ADP-ribose)- and PCNA-dependent mechanisms. *Nucleic Acids Res.* **39**, 5045-5056.

Nesvizhskii, A. I., Keller, A., Kolker, E. and Aebersold, R. (2003). A statistical model for identifying proteins by tandem mass spectrometry. *Anal. Chem.* **75**, 4646-4658.

Nykamp, K., Lee, M. H. and Kimble, J. (2008). C. elegans La-related protein, LARP-1, localizes to germline P bodies and attenuates Ras-MAPK signaling during oogenesis. *RNA* **14**, 1378-1389.

Ong, S. E. and Mann, M. (2007). Stable isotope labeling by amino acids in cell culture for quantitative proteomics. *Methods Mol. Biol.* **359**, 37-52.

Ong, S. E., Blagoev, B., Kratchmarova, I., Kristensen, D. B., Steen, H., Pandey, A. and Mann, M. (2002). Stable isotope labeling by amino acids in cell culture, SILAC, as a simple and accurate approach to expression proteomics. *Mol. Cell. Proteomics* **1**, 376-386.

Patel, C. N., Koh, D. W., Jacobson, M. K. and Oliveira, M. A. (2005). Identification of three critical acidic residues of poly(ADP-ribose) glycohydrolase involved in catalysis: determining the PARG catalytic domain. *Biochem. J.* **388**, 493-500.

Pleschke, J. M., Kleczkowska, H. E., Strohm, M. and Althaus, F. R. (2000). Poly(ADP-ribose) binds to specific domains in DNA damage checkpoint proteins. *J. Biol. Chem.* **275**, 40974-40980.

Rouleau, M., Aubin, R. A. and Poirier, G. G. (2004). Poly(ADP-ribosyl)ated chromatin domains: access granted. *J. Cell Sci.* **117**, 815-825.

Rouleau, M., Patel, A., Hendzel, M. J., Kaufmann, S. H. and Poirier, G. G. (2010). PARP inhibition: PARP1 and beyond. *Nat. Rev. Cancer* **10**, 293-301.

Saeed, A. I., Sharov, V., White, J., Li, J., Liang, W., Bhagabati, N., Braisted, J., Klapa, M., Currier, T., Thiagarajan, M. et al. (2003). TM4: a free, open-source system for microarray data management and analysis. *Biotechniques* **34**, 374-378.

Scott, G. S., Kean, R. B., Mikheeva, T., Fabis, M. J., Mabley, J. G., Szabó, C. and Hooper, D. C. (2004). The therapeutic effects of PJ34 [N-(6-oxo-5,6-dihydrophenanthridin-2-yl)-N,N-dimethylacetamide.HCl], a selective inhibitor of poly(ADP-ribose) polymerase, in experimental allergic encephalomyelitis are associated with immunomodulation. *J. Pharmacol. Exp. Ther.* **310**, 1053-1061.

Smith, B. C., Settles, B., Hallows, W. C., Craven, M. W. and Denu, J. M. (2011). SIRT3 substrate specificity determined by peptide arrays and machine learning. *ACS Chem. Biol.* **6**, 146-157.

Sugawara, T., Oguro, H., Negishi, M., Morita, Y., Ichikawa, H., Iseki, T., Yokosuka, O., Nakauchi, H. and Iwama, A. (2010). FET family proto-oncogene Fus contributes to self-renewal of hematopoietic stem cells. *Exp. Hematol.* **38**, 696-706.

Tourrière, H., Gallouzi, I. E., Chebli, K., Capony, J. P., Mouaikel, J., van der Geer, P. and Tazi, J. (2001). RasGAP-associated endoribonuclease G3Bp: selective RNA degradation and phosphorylation-dependent localization. *Mol. Cell. Biol.* **21**, 7747-7760.

Tourrière, H., Chebli, K., Zekri, L., Courselaud, B., Blanchard, J. M., Bertrand, E. and Tazi, J. (2003). The RasGAP-associated endoribonuclease G3BP assembles stress granules. *J. Cell Biol.* **160**, 823-831.

Tulin, A. and Spradling, A. (2003). Chromatin loosening by poly(ADP)-ribose polymerase (PARP) at Drosophila puff loci. *Science* **299**, 560-562.

Veuger, S. J., Curtin, N. J., Richardson, C. J., Smith, G. C. and Durkacz, B. W. (2003). Radiosensitization and DNA repair inhibition by the combined use of novel inhibitors of DNA-dependent protein kinase and poly(ADP-ribose) polymerase-1. *Cancer Res.* **63**, 6008-6015.

Wang, Y., Dawson, V. L. and Dawson, T. M. (2009). Poly(ADP-ribose) signals to mitochondrial AIF: a key event in parthanatos. *Exp. Neurol.* **218**, 193-202.

Wang, Y., Kim, N. S., Haince, J. F., Kang, H. C., David, K. K., Andrabi, S. A., Poirier, G. G., Dawson, V. L. and Dawson, T. M. (2011). Poly(ADP-ribose) (PAR) binding to apoptosis-inducing factor is critical for PAR polymerase-1-dependent cell death (parthanatos). *Sci. Signal.* **4**, ra20.

Yu, S. W., Andrabi, S. A., Wang, H., Kim, N. S., Poirier, G. G., Dawson, T. M. and Dawson, V. L. (2006). Apoptosis-inducing factor mediates poly(ADP-ribose) (PAR) polymer-induced cell death. *Proc. Natl. Acad. Sci. USA* **103**, 18314-18319.

Yung, T. M., Sato, S. and Satoh, M. S. (2004). Poly(ADP-ribosyl)ation as a DNA damage-induced post-translational modification regulating poly(ADP-ribose) polymerase-1-topoisomerase I interaction. *J. Biol. Chem.* **279**, 39686-39696.

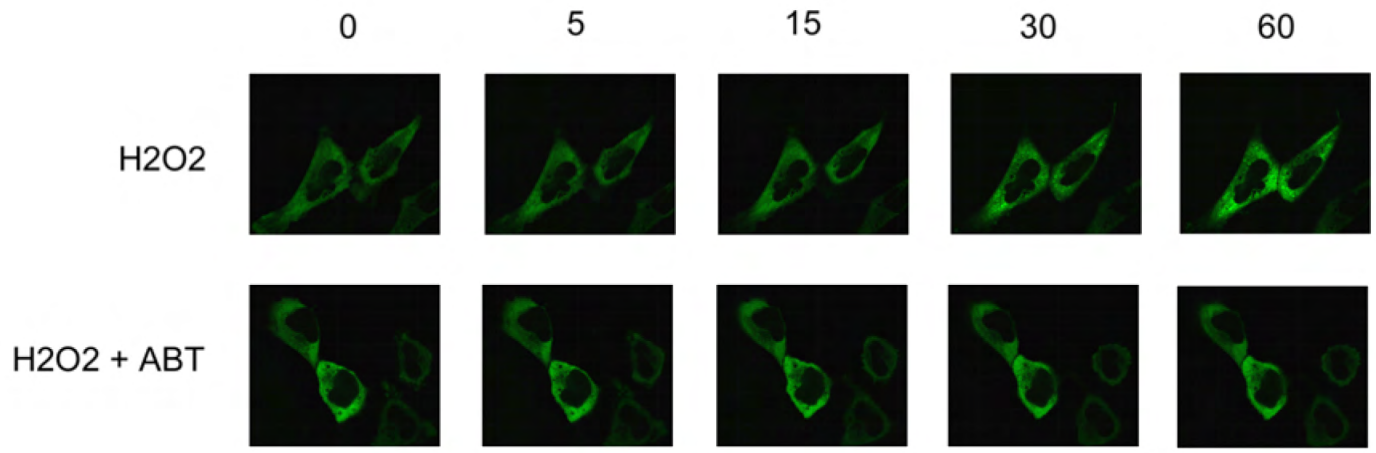

Fig. S1. Microscopy experiments with live cells reveal G3BP foci formation upon DNA damage.